

## Article

# A Partial Discharge Localization Method Based on the Improved Artificial Fish Swarms Algorithm

Hao Qiang <sup>1,2</sup> , Qun Wang <sup>1</sup>, Hui Niu <sup>1</sup>, Zhaoqi Wang <sup>1</sup> and Jianfeng Zheng <sup>1,2,\*</sup> <sup>1</sup> School of Mechanical Engineering and Rail Transit, Changzhou University, Changzhou 213164, China<sup>2</sup> Jiangsu Province Engineering Research Center of High-Level Energy and Power Equipment, Changzhou University, Changzhou 213164, China

\* Correspondence: zjf@cczu.edu.cn

**Abstract:** Accurate localization of partial discharge in GIS equipment remains a key focus of daily maintenance for substations, which can be achieved through advanced detection and location techniques, as well as regular maintenance and testing of the equipment. However, there is currently an issue with low accuracy in the localization algorithm. Aiming at the problems of low precision and local optimization of the swarm intelligence algorithm in partial discharge localization system of GIS equipment, this paper proposes a 3D localization algorithm based on a time difference of arrival (TDOA) model of the improved artificial fish swarm algorithm (IAFSA). By introducing the investigation behaviour of the artificial bee colony (ABC) algorithm into the artificial fish swarms algorithm (AFSA), this algorithm is more efficient to jump out of the local extremum, enhance the optimization performance, improve the global search ability and overcome the premature convergence. Furthermore, more precise positioning can be achieved with dynamic parameters. The results of the testing function show that IAFSA is significantly superior to AFSA and particle swarm optimization (PSO) in terms of positioning accuracy and stability. When applied to partial discharge localization experiments, the maximum relative positioning error is less than 2.5%. This validates that the proposed method in this paper can achieve high-precision partial discharge localization, has good engineering application value, and provides strong support for the safe operation of GIS equipment.

**Keywords:** AFSA; GIS equipment; partial discharge; precise localization

**Citation:** Qiang, H.; Wang, Q.; Niu, H.; Wang, Z.; Zheng, J. A Partial Discharge Localization Method Based on the Improved Artificial Fish Swarms Algorithm. *Energies* **2023**, *16*, 2928. <https://doi.org/10.3390/en16062928>

Academic Editors: Alistair Duffy and Antonella Ragusa

Received: 18 February 2023

Revised: 19 March 2023

Accepted: 21 March 2023

Published: 22 March 2023



**Copyright:** © 2023 by the authors. Licensee MDPI, Basel, Switzerland. This article is an open access article distributed under the terms and conditions of the Creative Commons Attribution (CC BY) license (<https://creativecommons.org/licenses/by/4.0/>).

## 1. Introduction

Gas-insulated switchgear (GIS) is widely used in electric power systems due to its advantages of small floor space, high reliability, long maintenance cycle, immunity from environmental pollution and high altitude [1,2]. In recent years, GIS equipment failure has occurred frequently. GIS equipment failure will not only cause complete shutdown or partial power failure of the substation, but also cause power loss, increase maintenance cost, affect PD reliability of the power grid, and pose a significant threat to the safe operation of the power grid [3]. When PD occurs inside GIS, electromagnetic wave signals are generated, radiating to the surrounding area. Moreover, electromagnetic wave signals have the characteristics of anti-electromagnetic solid interference and strong directionality, which provides a theoretical basis for the localization of PD [4]. The localization algorithm plays a crucial role in the localization of partial discharge [5–7].

There are several mature online monitoring techniques for partial discharge, such as the ultra-high-frequency detection method [8] and the ultrasonic detection method [9]. However, ultrasonic signals attenuate quickly during propagation in GIS and are susceptible to equipment vibration interference, making ultrasonic detection generally unsuitable for partial discharge in GIS [10]. The ultra-high-frequency detection method has strong anti-interference ability, high sensitivity, and is not affected by mechanical vibration, making it the main means of partial discharge online monitoring currently [11].

The methods for UHF-based partial discharge localization for GIS equipment usually include time of arrival (TOA), time difference of arrival (TDOA), and received signal strength (RSS). Ahmad Hafiz Mohd Hashim et al. [12] proposed a method for locating partial discharges (PD) in oil-filled equipment using acoustic emission (AE) and fuzzy logic. The method involves pre-processing data with discrete wavelet transform (DWT), analysing it with time of arrival (TOA), and applying fuzzy logic Mamdani (FLM) and Takagi–Sugeno (FLTS) methods to determine the distance between the PD and AE sensors. Ephraim Tersoo Iorkyase et al. [13] proposed a cost-effective radio fingerprinting technique. This technique uses the received signal strength (RSS) extracted from PD measurements gathered using RF sensors. The results demonstrated that the neural network produced superior performance as a result of its robustness against noise. The TDOA method based on UHF is the most widely used method for partial discharge localization in GIS equipment [14–16].

During the PD source localization process, the TDOA method is first used to establish a non-linear system of equations based on the different time delays of the electromagnetic wave signals arriving at the receiving antennas. The non-linear system is then iteratively solved using non-linear optimization methods to obtain the accurate location of the PD source. The methods for finding the optimal solution in solving the equations include PSO [17], least squares method [18], genetic algorithm [19] and other methods. Traditional algorithms are computationally complex and require careful selection of the initial values. When the initial values are not properly chosen, the localization result may not converge or even diverge.

The traditional PD source localization algorithm often fails to provide the correct position of the PD, so some researchers have improved it using intelligent algorithms. Meka et al. [20] adjusted the inertia weight of PSO effectively by using 49 and 9 simple IF-THEN fuzzy rules to improve the global optimal solution, weaken the local convergence problem and improve accuracy when estimating the PD source position. Xiaoxing Zhang et al. [21] proposed a PD location method based on the Taylor–genetic algorithm. The Taylor expansion method is used to solve hyperbolic equations, and the genetic algorithm is utilized to search for the optimal initial point. The results show that using the genetic algorithm to find an appropriate initial point greatly enhances the feasibility of the Taylor algorithm. Junyi Cai et al. [22] proposed a hybrid DE-PSO algorithm by combining the advantages of the differential evolution (DE) algorithm and the particle swarm optimization (PSO) algorithm, which can maintain great diversity even at the later stages of the calculation. The simulation and experimental results showed that the proposed algorithm has excellent performance with high accuracy and strong robustness, and it can meet the needs of field applications. Sourav Dhara et al. [23] proposed a near-field-based approach for localization of PD sources with the help of a TDOA scheme. The result indicates the superiority of the proposed near-field-based approach. Agostino Forestiero [24] proposed a heuristic method that utilizes swarm intelligence techniques to construct a recommender engine in an IoT environment. The method represents smart objects using real-valued vectors obtained through the Doc2Vec model and employs a bio-inspired model, the flocking model, to perform simple and local operations autonomously to achieve global intelligent organization. A similarity rule based on the assigned vectors is designed to cluster similar agents. The intelligent positioning allows for easy identification of similar smart objects, thus enabling fast and effective selection operations. Experimental results demonstrate that the proposed method improves clustering quality and relevance performance by about 50%. Agostino Forestiero et al. [25] proposed a multi-agent-based approach for spatial sorting and discovery of resource information provided by Grid. The behaviour of these agents is inspired by ant colonies, and they can replicate or simply relocate resource descriptors. By setting parameters similar to the ant pheromone mechanism, the balance between these two objectives can be adjusted. The balance can be either static or dynamic. In the latter case, a “epidemic” mechanism is used to convey the value of this parameter to the hosts and agents of the Grid. Simulation analysis confirms the effectiveness of the reorganization and discovery protocols as well as the aforementioned virus adjustment mechanism.

The traditional AFSA algorithm optimizes and solves problems through four behaviours, but it is prone to getting stuck in local optimal solutions. Although it can obtain an approximate global optimal solution, its search horizon and step size are fixed, which can lead to premature convergence and reduce global optimization ability. To address these issues and leverage the characteristics of AFSA, an AFSA algorithm with adaptive parameters to improve the search horizon and step size is proposed. Increasing the search horizon and step size in the early stage of the algorithm can help it quickly discover potential optimal or better solutions and avoid getting stuck in local optimal solutions. As the search progresses, the algorithm gradually reduces the size of the search horizon and step size to finely search the search space, further improving the convergence performance and search accuracy of the algorithm. This adaptive strategy can improve the search efficiency and accuracy of the algorithm, avoid it becoming stuck in local optimal solutions, and ensure that the algorithm searches for the optimal solution in the global scope. Optimization improvements in algorithms can enhance the accuracy of partial discharge localization when applied.

Therefore, we conducted research on intelligent algorithms for partial discharge localization and proposed a three-dimensional localization algorithm based on a TDOA model using an IAFSA algorithm. The main steps include the following: Firstly, it is necessary to construct a mathematical model of the GIS physical entity and partial discharge for subsequent calculations. We acquire and pre-process partial discharge ultra-high-frequency electromagnetic wave data using an oscilloscope. Secondly, we use the generalized cross-correlation algorithm to calculate the delay of partial discharge and obtain the delay data of each receiving antenna. Thirdly, we input the delay data into the IAFSA to solve the localization of the partial discharge source. The main contributions are as follows:

- (1) The algorithm introduces exploration behaviour based on the traditional artificial bee colony algorithm, making the algorithm more globally optimal and avoiding becoming stuck in local optimal solutions by introducing new random factors.
- (2) The algorithm uses dynamic parameters to adjust the value of parameters according to the search process to more accurately locate the partial discharge source.
- (3) We build an experimental platform and conduct on-site experiments to verify the practical application effectiveness of our algorithm in engineering.

## 2. Principle of PD Localization

### 2.1. Mathematical Model

For the localization problem of the local PD, the TDOA is often used to obtain non-linear equations. However, direct solving has high requirements for the iterative convergence of the equations. Due to the influence of various interference noises, measurement error, and other factors, there is no solution or multiple solutions, so this paper transforms the problem of solving equations into an optimization problem. The main principle of electromagnetic wave positioning [26] is as follows:

- (1) collect the electromagnetic wave signals with a four-channel sensor;
- (2) convert these signals into the time delay signals by the TDOA algorithm;
- (3) substitute these signals into a mathematical model of electromagnetic wave positioning to solve the location of the partial discharge points. The GIS equipment is equivalent to a cylinder, and the spatial Cartesian coordinate system is established as shown in Figure 1.

Where,  $P(x_p, y_p, z_p)$  is the partial discharge point, and  $S_i(x_i, y_i, z_i)$  ( $i = 1, 2, 3, 4$ ) represent the sensors.  $S_1$  is used as a reference sensor. According to Figure 1, the relative distance difference between  $S_2, S_3, S_4$  and  $S_1$  to  $P$  can be expressed as:

$$\Delta l_i = \sqrt{(x_i - x_p)^2 + (y_i - y_p)^2 + (z_i - z_p)^2} - \sqrt{(x_1 - x_p)^2 + (y_1 - y_p)^2 + (z_1 - z_p)^2} \quad (1)$$

where  $i = 2, 3, 4$ .

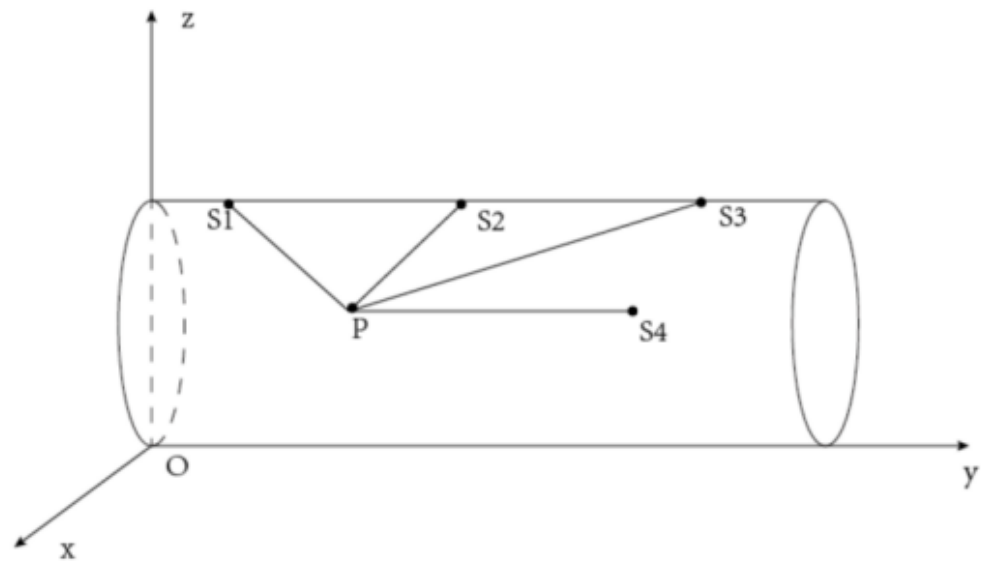


**Figure 1.** Localization model of GIS equipment.

The time delay between an electromagnetic wave received by  $S_i$  and  $S_1$  is labelled as  $\tau_{i1}$  ( $i = 2, 3, 4$ ). Therefore,  $\Delta l_{i1} \approx \tau_{i1}v$ , and  $v$  is the speed of the electromagnetic wave. Subsequently, the following fitness function  $f$  can be obtained

$$f(x_p, y_p, z_p) = \sum_{i=2}^4 (\Delta l_{i1} - \tau_{i1}v) \quad (2)$$

Equation (2) is a non-linear equation, and it is difficult to be solved directly. To simplify the calculation, it can be equivalent to an optimization problem with constraints, expressed as

$$\begin{cases} \min f(x_p, y_p, z_p) \\ -r \leq x_p \leq r \\ 0 \leq y_p \leq l \\ 0 \leq z_p \leq 2r \end{cases} \quad (3)$$

where  $l$  and  $r$  represent the length and radius of the GIS equipment, respectively.

## 2.2. Calculation of the Time Delay Based on the TDOA

Assuming that the partial discharge source transmits a high-frequency (HF) signal at time  $T_0$ ,  $S_1$  and  $S_2$  receive the signal after  $T_1$  and  $T_2$ , respectively, as shown in Figure 2. Therefore, the time difference between them can be calculated as:

$$\tau_{21} = T_2 - T_1 \quad (4)$$

Compared with simulation, the time difference is difficult to be calculated directly by Equation (4) in the actual project, mainly for the following reasons:

- (1) The HF signal contains a lot of environmental noises, and it is difficult to distinguish the starting point of the signal directly.
- (2) In terms of the signal transmission speed and distance between the sensors, the time difference is at the nanosecond level and the calculation accuracy is thus required to be high. Therefore, in practical applications, it is necessary to find more effective time delay calculation methods to ensure the accuracy of PD location.

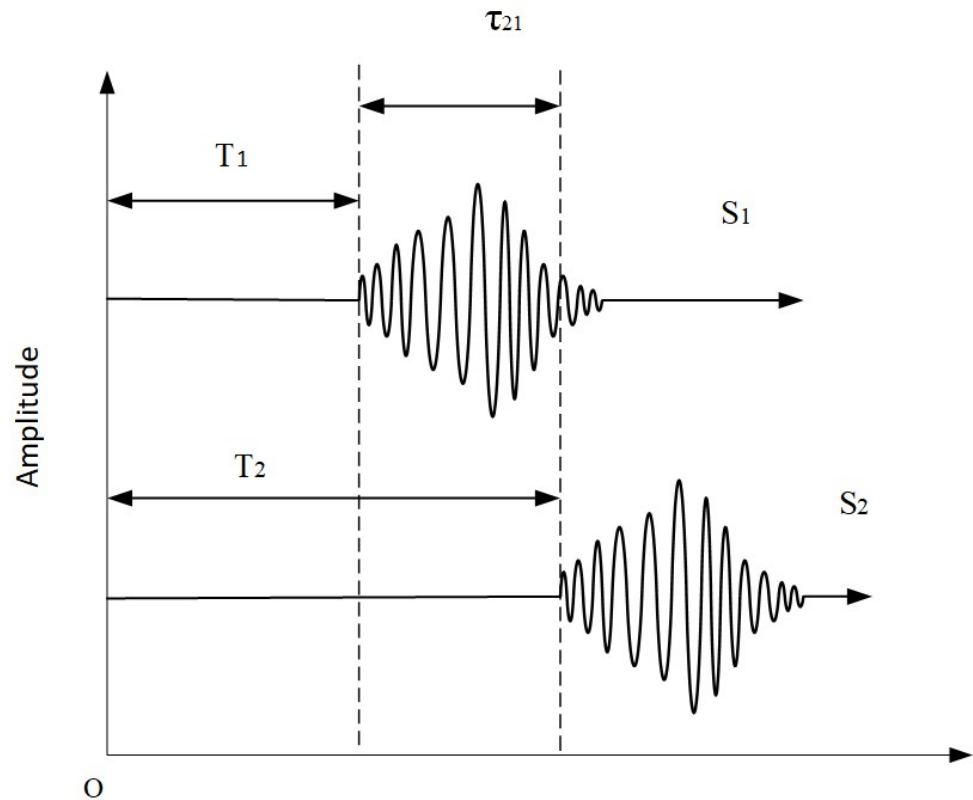


**Figure 2.** Schematic diagram of the time delay calculation.

### 2.3. Generalized Cross-Correlation

Cross-correlation (CC) [27,28] is a method to compare the similarity of two functions or signals in the time domain, which can estimate the time delay using the correlation functions of two independently received signals,  $x_1(t)$  and  $x_2(t)$ .

$$\begin{cases} x_1(t) = s(t) + n_1(t) \\ x_2(t) = s(t - D) + n_2(t) \end{cases} \quad (5)$$

where  $s(t)$  represents the target source signal.  $n_1(t)$  and  $n_2(t)$  stand for two independent background noises.  $D$  is the relative time delay of signal  $x_1(t)$  and  $x_2(t)$ , which can be positive or negative.

Figure 3 shows the flow of generalized cross-correlation algorithm (GCC).  $x_1(t)$  and  $x_2(t)$  are two different input signals, such as the partial discharge signals measured by two sensors at different locations.  $H_1(f)$  and  $H_2(f)$  are filter functions. The correlator is to calculate the CC function between the two pre-processed signals  $y_1(t)$  and  $y_2(t)$ . The time value corresponding to the peak value of the CC function is the time delay estimation. In fact, the GCC is the Fourier transforms weighted by the cross power spectrum of the input signal.

According to the Wiener–Khinchin’s theorem, the CC function and its cross power spectrum are Fourier transform pairs of each other:

$$R_{x_1x_2}(\tau) = F^{-1}[G_{x_1x_2}(\omega)] \quad (6)$$

$$R_{y_1y_2}(\tau) = F^{-1}[G_{y_1y_2}(\omega)] \quad (7)$$

$y_1(t)$  and  $y_2(t)$  are the filtering results of  $x_1(t)$  and  $x_2(t)$ . Such that:

$$\begin{aligned} R_{y_1 y_2}(\tau) &= F^{-1}[G_{y_1 y_2}(\omega)] \\ &= F^{-1}[G_{x_1 x_2}(\omega)H_1(\omega)H_2^*(\omega)] \end{aligned} \quad (8)$$

where  $(H_1(\omega)H_2^*(\omega))$  is the weighted coefficient, which affects the accuracy of the time delay estimation. This paper adopts the Hassab–Boucher (HB) weighting method, and the weighting function is  $|G_{x_1 x_2}|(G_{x_1 x_1}G_{x_2 x_2})^{-1}$ . HB weighting has an inhibitory effect on the periodic component of the signal, and the effect of low SNR is the same as the direct CC method; therefore, the estimation accuracy is higher.

By obtaining the time delay, we can use optimization algorithms, such as IAFSA, to solve for the coordinates of the partial discharge source.

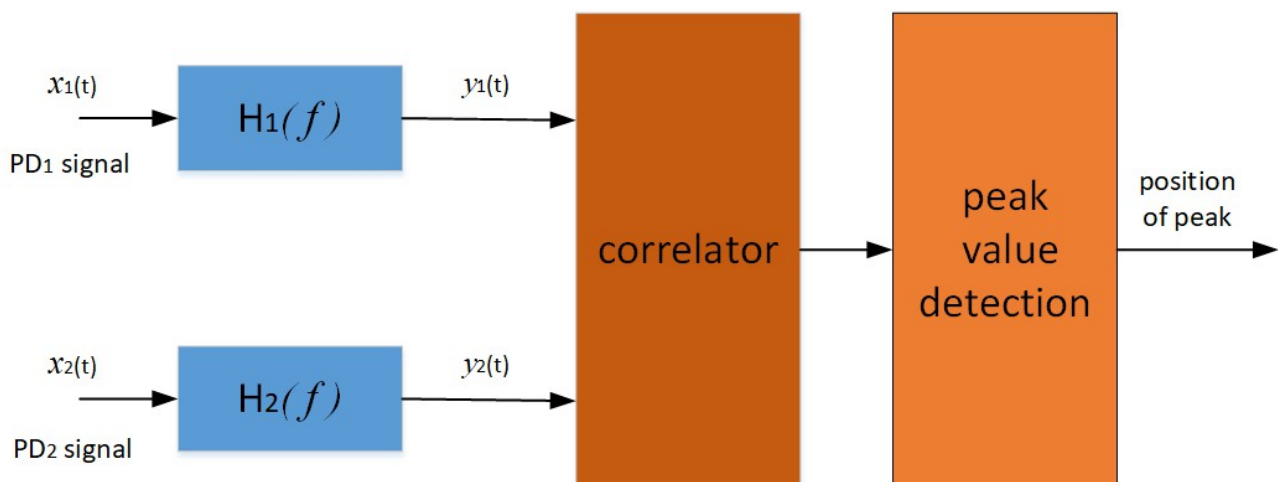


**Figure 3.** Flowchart of generalized cross-correlation algorithm.

### 3. Improved AFSA

The AFSA [29–32] is an artificial intelligence algorithm realized by simulating the group behaviour of natural organisms. It adopts a bottom-up approach and a behaviour-based artificial intelligence method. The idea is that, for example, in water fish tend to find the highest concentrations of food and flock towards them. Therefore, by simulating the daily behaviour of fish, it is possible to find the location with the highest food concentration, namely, the optimal solution.

#### 3.1. Adaptive Vision Field and Step Length

##### 3.1.1. Adaptive Vision Field

AFSA has the advantages of a good global parallel ability, simple structure, and fast convergence speed in the early stages. However, it also has the disadvantages of slower convergence speeds in the late stages and can easily fall into a local optimum. When applied to PD localization, the accuracy is low. Concerning its slow convergence speed in the later stages, this paper adopts adaptive parameters, with smaller adaptive parameters in the later iteration process to not only enhances convergence speed, but to also improve the optimization accuracy.

In the traditional AFSA, the vision field and step length of artificial fish are fixed when they perform praying, swarming and following, which decreases the search accuracy and affects the convergence speed. The specific performance is as follows: the larger the field of vision, the stronger the global search ability with a faster convergence speed, while when the field of vision is smaller, the local search ability becomes stronger. The larger the step length, the faster the convergence speed, but there may be an oscillation phenomenon. However, as the step length becomes smaller, the convergence speed tends to slow, but with higher accuracy. Figure 4 shows the schematic diagram of the vision field  $Visual_k$  and step length  $Step_k$ . When the food concentration at position  $f_a$  in the vision field is greater than

that at the current position  $f_m$ , the artificial fish will step forward to  $f_{next}$ . Otherwise, the fish will search for other locations, such as  $f_b$  and  $f_c$ .

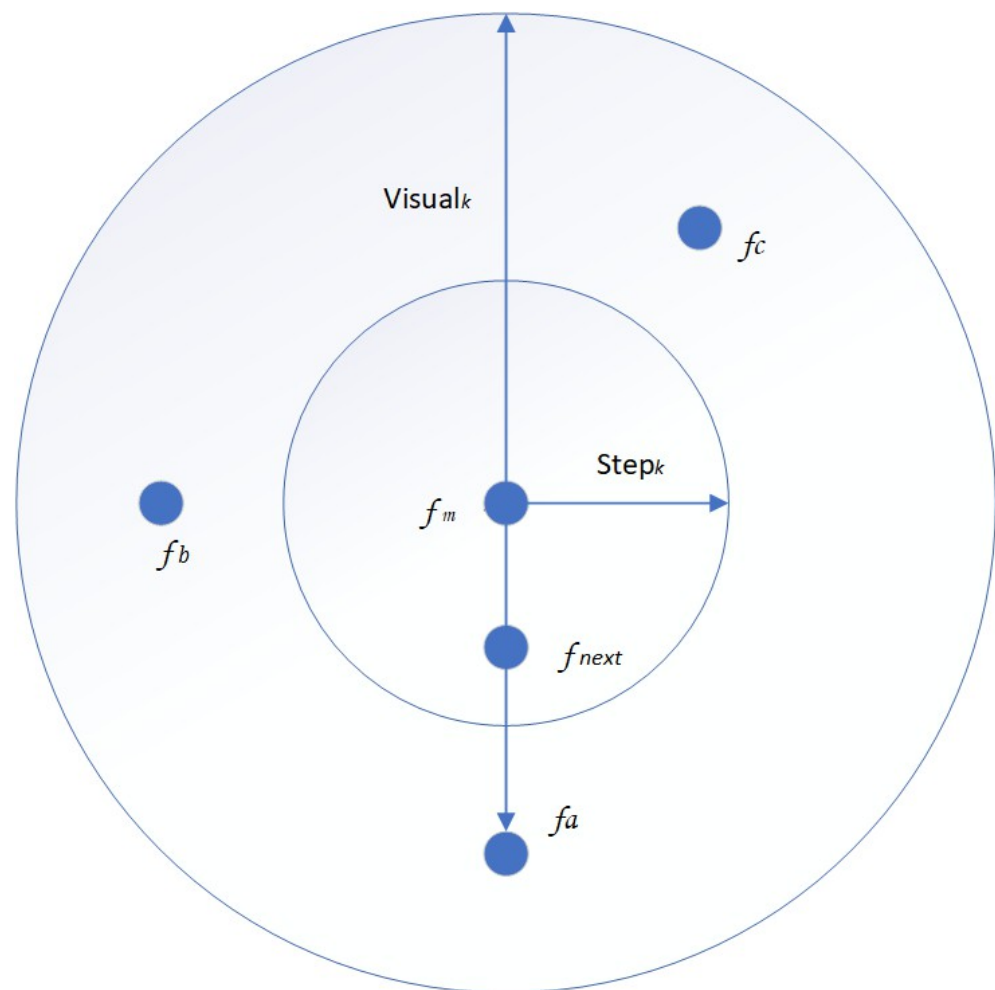


**Figure 4.** Vision field and step length of artificial fish.

Therefore, in the early stages the convergence speed and search-ability of the global optimal solution are improved by enlarging the vision field and step length. In the middle stage, the vision field and step length are gradually reduced to find the local optimal solution. In the late stage, the vision field and step length are reduced to a minimum, and the search is focused in the remaining small area. The improved updated formula of the vision field could be expressed as:

$$Visual_k = \left( \frac{1}{k} + \frac{1}{k+1} \right) Visual_k \quad (9)$$

where  $k$  is the number of the current iteration.

When fish choose a behaviour, they usually choose the prey behaviour. Considering this characteristic, we only need to adjust the related mechanism of the prey behaviour. The fish obtain a reasonable vision field in the early stage, and this decreases with the optimization iterations. As a result, the dynamic changing of the vision field based on the number of iterations is helpful to carry out an accurate local search in the neighbourhood of the optimal solution. The adaptive change of the vision field makes the algorithm have a faster optimization speed and ensures the accuracy of the final optimal solution.

### 3.1.2. Adaptive Step Length

In the traditional AFSA, the individual fish moves forward with a fixed step length, often leading the later iterative solution to fall into a local optimum which is difficult to jump out. To avoid such a situation and to balance the stability and efficiency of the algorithm, this paper adopts an adaptive step length, expressed as:

$$Step_k = \left(\frac{1}{k} - \frac{1}{k+1}\right) Step_k \quad (10)$$

where  $k$  is the number of the current iteration.

The improved pray behaviour based on an adaptive step length ensures the optimal individual fish can participate in the next iteration, and the sub-optimal individual fish can participate in the next iteration with a certain probability. The updated sub-optimal individual fish makes the fish jump out from the local optimum to select the next round of behaviour, and finally achieve the global optimal solution.

## 3.2. Behaviour Description of the IAFSA

### 3.2.1. Improved Pray Behaviour

When praying, the current position and food concentration of the fish are labelled as  $f_m$  and  $F_m$ , respectively. Furthermore, within the perceptual range of the fish, a random point is selected and marked as  $f_n$  with the food concentration  $F_n$ . When  $F_n > F_m$ , the fish advances one step towards  $f_n$ . Otherwise, the state  $f_n$  is randomly re-selected for the subsequent judgment. After repeating *trynumber* times, if the updated condition is still not met, the investigation behaviour is carried out.

The update formula for the pray behaviour is expressed as:

$$f_{next} = \begin{cases} f_m + Rand \cdot Step_k \cdot \frac{f_n - f_m}{\|f_n - f_m\|} & F_n \geq F_m \\ \text{Investigational Behavior} & F_n < F_m \end{cases} \quad (11)$$

where *Rand* is a random number of (0,1) and  $\|f_n - f_m\|$  is the distance between  $f_n$  and  $f_m$ .  $f_{next}$  represents the the next position of the fish.

### 3.2.2. Improved Swarm Behaviour

When swarming, within the perceptual range of the fish, there are  $n_f$  partners and the centre position of these partners is  $f_c$  with the food concentration  $F_c$ .  $F_c/n_f > \delta F_m$  indicates that there is more food at  $f_c$  and its surroundings are not crowded, then the fish moves one step towards  $f_c$ . Otherwise, the pray behaviour is carried out. The update formula for the swarm behaviour is:

$$f_{next} = \begin{cases} f_m + Rand \cdot Step_k \cdot \frac{f_c - f_m}{\|f_c - f_m\|} & \frac{F_c}{n_f} \geq \delta F_m \\ \text{Pray Behavior} & \frac{F_c}{n_f} < \delta F_m \end{cases} \quad (12)$$

where  $\delta$  represents the crowding factor, and  $n_f$  is the fish partners.

### 3.2.3. Improved Follow Behaviour

When following, once a fish has found that food is abundant around its partner, it will follow the optimal partner  $f_{max}$  with the food concentration  $F_{max}$  and move closer to  $f_{max}$ . If  $F_{max}/n_f > \delta F_m$ , then there is a higher food concentration at  $F_{max}$  and its surroundings are not crowded, and the fish advances one step towards  $f_{max}$ . Otherwise, the pray behaviour is executed.

The update formula for the follow behaviour can be expressed as:

$$f_{next} = \begin{cases} f_m + Rand \cdot Step_k \cdot \frac{f_{max} - f_m}{\|f_{max} - f_m\|} & \frac{F_{max}}{n_f} \geq \delta F_m \\ Pray Behavior & \frac{F_{max}}{n_f} < \delta F_m \end{cases} \quad (13)$$

where  $f_{max}$  is the position coordinate of the partner with the optimal state.

### 3.2.4. Improved Investigation Behaviour

Although AFSA has a fast convergence in the initial optimization stage, it is easy to fall into a local optimum. Concerning this problem, this paper introduces a detection mechanism of the ABC algorithm into the AFSA [33–35]. In the fish population, the fish with the poorest fitness value is defined as the detecting fish, and its position is reassigned to realize the re-optimal search in the search space. The random behaviour of the AFSA is replaced by the detection behaviour, and the higher local optimization ability of the ABC detection mechanism is used to make up for the shortages of the AFSA. As a result, the fish swarm can accelerate the convergence in the optimization process, are better able to jump out of the local optimum, and avoid the premature problem. The calculation formula for the investigation behaviour is:

$$f_{next} = f_{best} + Rand \cdot (f_m - f_{best}) \quad (14)$$

where  $f_{best}$  is the coordinate of the corresponding fish in the bulletin board.

### 3.3. Flow of the IAFSA

As is shown in Figure 5, the main steps for locating the PD using the IAFSA are as follows:

Step 1: Coordinated values and arrival delay of the four sensors are input;

Step 2: The initialization parameters, including the maximum number of iterations  $K_{max}$ , the population size  $N$ , the initial position of each fish (the coordinate value of the PD source), the initial vision field  $Visual_1$ , the initial step length  $Step_1$ , the crowding factor  $\delta$ , and the number of repetitions  $trynumber$  are set;

Step 3: The fitness value of each individual of the initial fish swarm is calculated, and the optimal fitness value in the bulletin board is recorded;

Step 4: The adaptive  $Visual_k$  and  $Step_k$  is calculated according to the number of iterations;

Step 5: The swarm and follow behaviours are executed; furthermore, the pray or investigation behaviours are performed according to the food concentration condition;

Step 6: The fitness values of the pray, follow, investigation and swarm behaviour are compared with the fitness values of the bulletin board to replace or retain the fitness values of the bulletin board;

Step 7: The iteration according to  $K_{max}$  or the convergence condition are stopped or repeated;

Step 8: The position coordinates of the PD source are output.

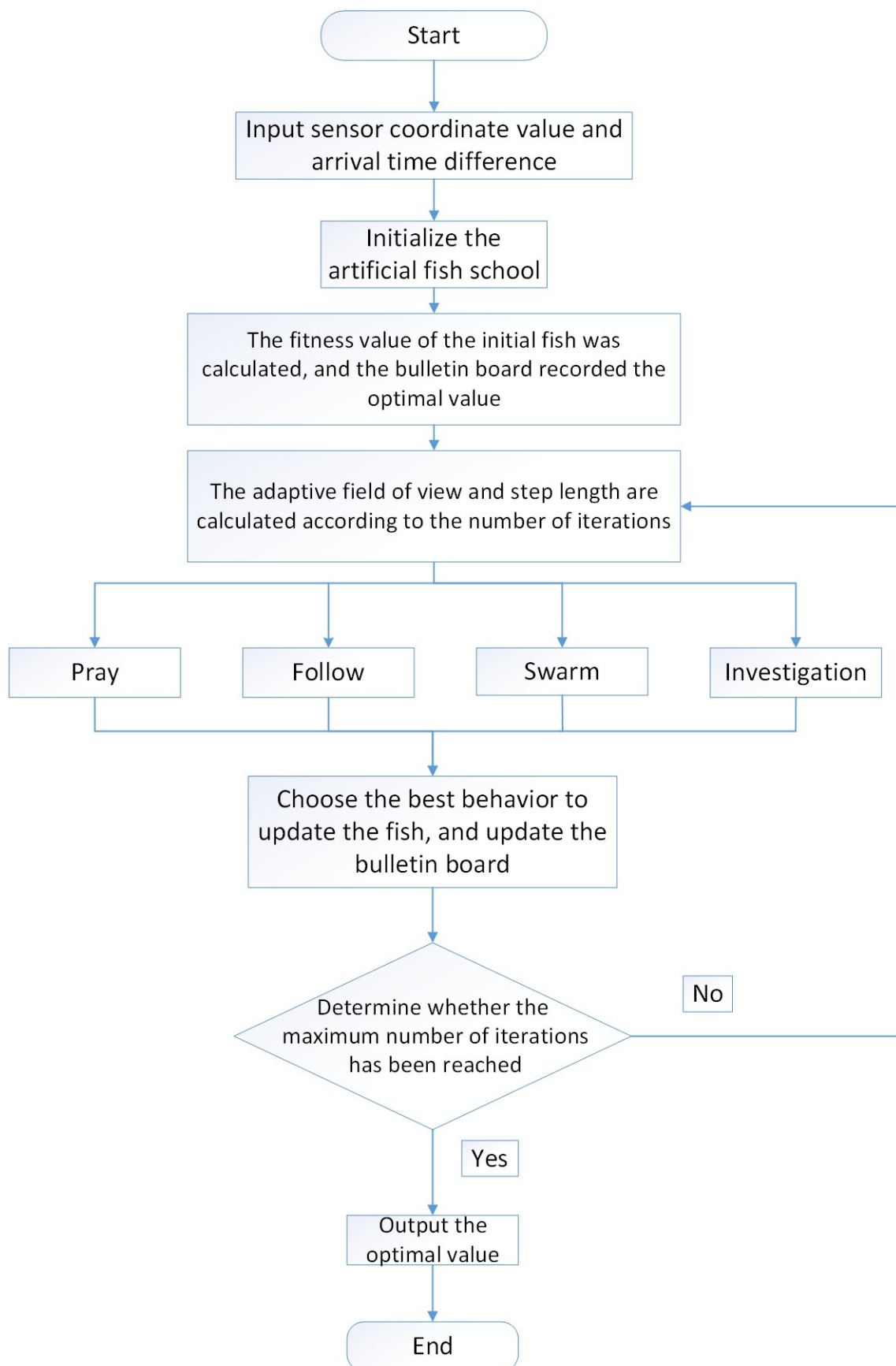


Figure 5. Flowchart of the IAFSA.

### 4. IAFSA Simulation Test

#### Standard Test Function and Simulation Test

In order to evaluate the performance of the IAFSA, 12 standard test functions were selected to carry out 50 experiments, and the results were compared with those of the AFSA and PSO. The experimental results less than  $10^{-8}$  are represented by 0. The experimental environment used MATLAB 2018a, Windows 11, and an Intel(R) Core(TM) i5-12500H @ 3.1 GHz CPU with 16 GB of RAM. Table 1 shows the selected test functions, where Dim denotes the number of variables. These functions are derived from the CEC benchmark function [36], covering unimodal functions (F<sub>1</sub>–F<sub>4</sub>), multimodal functions (F<sub>5</sub>–F<sub>8</sub>), and fixed dimensional multimodal functions (F<sub>9</sub>–F<sub>12</sub>), all of which have minimum values. We set the PSO population size  $m = 50$ , maximum number of iterations  $k_{max} = 100$ , particle position range  $x_i \in [0, 255]$ , velocity range  $v_i \in [-10, 10]$ , individual learning factor  $c_1 \in [0.5, 2.5]$ , and social learning factor  $c_2 \in [0.5, 2.5]$ . The main simulation parameters of the AFSA and IAFSA were set as  $K_{max} = 100$ ,  $N = 100$ ,  $Visual_1 = 0.5$ ,  $Step_1 = 0.25$ ,  $\delta = 0.618$ , and  $trynumber = 100$ .

Table 1. Benchmark function.

Test Function	Type	Dim	Range	$f_{min}$
$F_1(x) = \sum_{i=1}^n x_i^2$	US	30	[-100, 100]	0
$F_2(x) = \sum_{i=1}^n  x_i  + \prod_{i=1}^n  x_i $	US	30	[-10, 10]	0
$F_3(x) = \sum_{i=1}^n ( x_i + 0.5 )^2$	US	30	[-100, 100]	0
$F_4(x) = \sum_{i=1}^n ix_i^4 + random(0, 1)$	US	30	[-128, 128]	0
$F_5(x) = -20exp(-0.2\sqrt{\frac{1}{n}\sum_{i=1}^n x_i^2}) - exp(\frac{1}{n}\sum_{i=1}^n cos(2\pi x_i)) + 20 + e$	UN	30	[-32, 32]	0
$F_6(x) = \frac{1}{4000}\sum_{i=1}^n x_i^2 - \prod_{i=1}^n cos(\frac{x_i}{\sqrt{i}}) + 1$	UN	30	[-600, 600]	0
$F_7(x) = \frac{\pi}{n}(10sin(\pi y_1) + \sum_{i=1}^{n-1}(y_i - 1)^2(1 + 10sin^2(\pi y_{i+1}))) + (y_n - 1)^2 + \sum_{i=1}^n u(x_i, 10, 100, 4)$	UN	30	[-50, 50]	0
$F_8(x) = 0.1(sin^2(3\pi x_1) + \sum_{i=1}^n (x_i - 1)^2(1 + sin^2(3\pi x_i + 1))) + (x_n - 1)^2(1 + sin^2(2\pi x_n)) + \sum_{i=1}^n u(x_i, 5, 100, 4)$	UN	30	[-50, 50]	0
$F_9(x) = 4x_1^2 - 2.1x_1^4 + \frac{1}{3}x_1^6 + x_1x_2 - 4x_2^2 + 4x_2^4$	FDM	2	[-5, 5]	-1.0316
$F_{10}(x) = (x_2 - \frac{5.1}{4\pi^2}x_1^2 + \frac{5}{\pi}x_1 - 6)^2 + 10(1 - \frac{1}{8\pi})cosx_1 + 10$	FDM	2	[-5, 5]	0.398
$F_{11}(x) = (1 + (x_1 + x_2 + 1)^2(19 - 14x_1 + 3x_1^2 - 14x_2 + 6x_1x_2 + 3x_2^2)) \times (30 + (2x_1 - 3x_2)^2 \times (18 - 32x_1 + 12x_1^2 + 48x_2 - 36x_1x_2 + 27x_2^2))$	FDM	2	[-2, 2]	3
$F_{12}(x) = 20 + x_1^2 + x_2^2 - 10cos(2\pi x_1) - 10cos(2\pi x_2)$	FDM	2	[-5.12, 5.12]	0

From Table 2, the mean value solved by the IAFSA is very close to the real value, while those solved by the AFSA and PSO deviate far from the real value because a few particles fall into the local optimum. In terms of the variance, the results solved by the IAFSA are close to zero, indicating that the results are stable. In contrast, the results of the AFSA and PSO are slightly more prominent. Clearly, the stability of the IAFSA is stronger than the AFSA or PSO.

To further investigate the performance of the IAFSA in standard function testing, we randomly selected an optimization process and studied the iterative process of the three algorithms. As shown in Figure 6, the optimization process used the standard test function F<sub>12</sub>. From the figure, it can be seen that the PSO algorithm was trapped in a local optimum near the fitness value of one and hovered around the local optimum value from the fifth generation to the fiftieth generation. Even in the final stage of optimization, the PSO algorithm failed to find the local optimum value, producing a large error. Although the AFSA did not fall into a local optimum, it only found the optimal value at the thirtieth generation, and there was still errors present compared to the optimal value. In contrast, the IAFSA

found the optimal value at the tenth generation and did not fall into a local optimum. This demonstrates that the IAFSA not only has the excellent ability to escape from local optima, but also has a fast convergence speed and a high convergence accuracy. In conclusion, the experimental results show that the IAFSA is an optimization algorithm with superior optimization performance, high stability, and a strong global convergence ability.

**Table 2.** Result of the benchmark function test (each function was executed 50 times).

Function	Mean (PSO)	Std (PSO)	Mean (AFSA)	Std (AFSA)	Mean (IAFSA)	Std (IAFSA)
$f_1$	$7.23 \times 10^{-5}$	$6.30 \times 10^{-5}$	$8.53 \times 10^{-5}$	$7.28 \times 10^{-5}$	<b>0</b>	<b>0</b>
$f_2$	0.23241	$8.23 \times 10^{-2}$	0.21362	$7.59 \times 10^{-2}$	<b>0</b>	<b>0</b>
$f_3$	5.61222	0.73845	3.58941	0.58127	<b>0</b>	<b>0</b>
$f_4$	0.69190	0.21219	0.82459	0.35841	<b>0.00069</b>	<b>0.00055</b>
$f_5$	2.10830	0.27572	2.00581	0.22584	<b>0</b>	<b>0</b>
$f_6$	0.00105	0.00168	0.02584	0.01265	<b>0</b>	<b>0</b>
$f_7$	4.41429	1.81612	1.58412	0.75614	<b>0.03541</b>	<b>0.01594</b>
$f_8$	0.50179	0.24452	0.25841	0.15847	<b>0</b>	<b>0</b>
$f_9$	-1.0316	0	-1.0316	0	-1.0316	<b>0</b>
$f_{10}$	0.39789	<b>0</b>	0.39789	<b>0</b>	0.39766	$3.58 \times 10^{-2}$
$f_{11}$	3	0	3	0	3	<b>0</b>
$f_{12}$	0.216845	0.143549	0.207093	0.141906	<b>0.000432</b>	<b>0</b>

The bolded content in the table indicates the best experimental results.

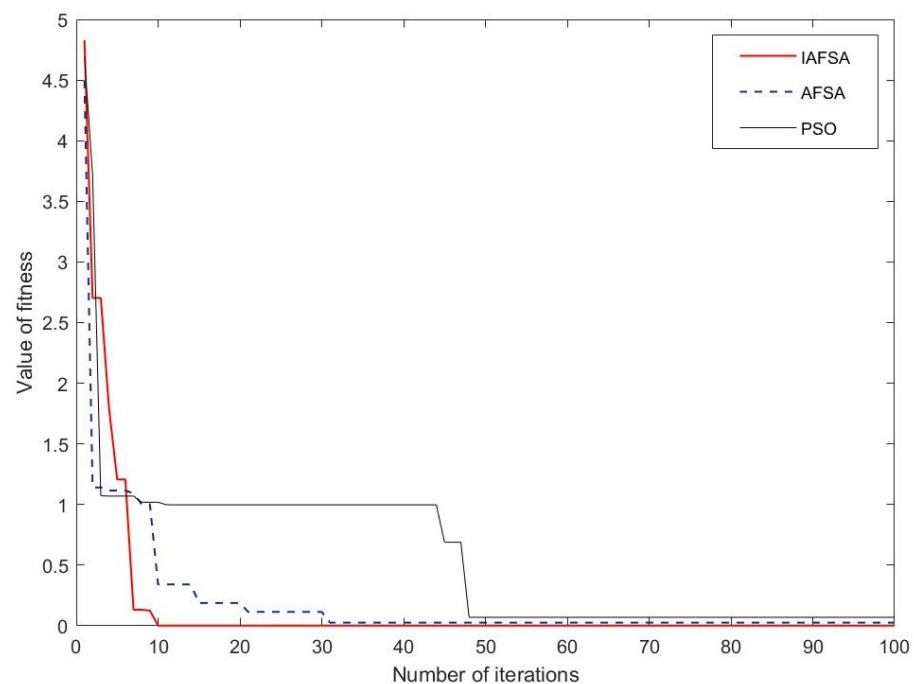


**Figure 6.** Convergence curve of test function  $F_{12}$ .

### 5. IAFSA for Simulation in the PD Location

To verify the practical effect of the IAFSA, a series of tests on the PD location were carried out on a 220 kV three-phase double-winding oil-immersed transformer by referring to the test data in [37]. As show in Figure 7, the dimensions of the transformer are:  $5000 \times 2500 \times 3000$  mm. The coordinates of the four sensors are  $S_1$  (3530,200,1620),  $S_2$  (1080,200,680),  $S_3$  (2310,200,430), and  $S_4$  (4340,200,680), with the coordinate unit in mm. The positions  $P$  of the PD sourced are shown in Table 3:

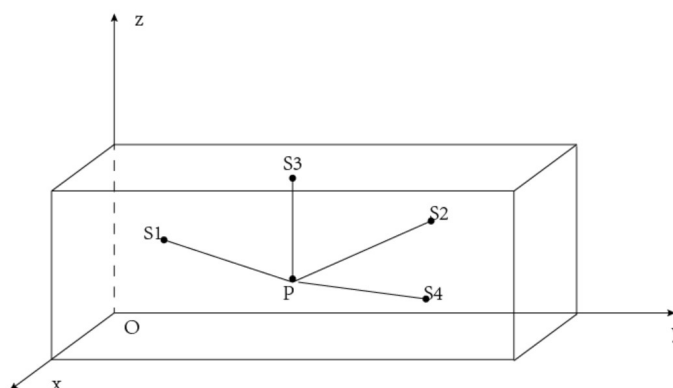


Figure 7. PD localization diagram.

Table 3. Standard test functions.

PD Source	Coordinate/mm	Measured Delay/ns
1	(1120,560,1300)	−9.07, −4.88, 4.12
2	(1120,520,2160)	−5.12, −2.01, 5.33
3	(2750,550,1300)	4.05, 0.40, 4.10
4	(3920,830,2150)	11.63, 7.71, 3.75
5	(4610,360,1480)	12.96, 7.55, −1.44

The main parameters of PSO, AFSA and IAFSA are shown in Table 4.

Table 4. Parameter settings of each algorithm for simulation.

Algorithm	$K_{max}$	N	Step <sub>1</sub>	Visual <sub>1</sub>	$\delta$	trynumber	$\omega$	$c_1 = c_2$
PSO	60	80	—	—	—	—	0.6	2
AFSA	60	80	10	5	0.618	30	—	—
IAFSA	60	80	10	5	0.618	30	—	—

If  $P(x,y,z)$  and  $P(x_i,y_i,z_i)$  are respectively represent the actual and calculated positions of the PD source, the distance error  $\Delta_r$  is defined as

$$\Delta_r = \sqrt{(x_i - x)^2 + (y_i - y)^2 + (z_i - z)^2} \tag{15}$$

In order to more clearly evaluate the performance of the positioning algorithm, this paper uses relative error as the evaluation index. The relative error refers to the difference between the actual positioning result and the furthest true position, calculated with the furthest true position as the reference. The specific calculation formula is as follows:

$$\delta_r = \frac{|\Delta_r|}{D_{dia}} \tag{16}$$

where  $D_{dia}$  is the distance between the two furthest points.

The smaller the relative error, the more accurate the positioning result. In practical applications, a relative error of less than 5% is considered a desirable positioning effect. By analysing and comparing the experimental data, the performance of different positioning algorithms can be evaluated, providing references for practical applications.

Through a series of simulated field tests, some conclusions could be achieved as follows:

The localization results of the IAFSA are global with location errors significantly less than the AFSA and PSO, as well as slightly less than the complex domain Newton iteration-grid search method (CDNIGS). Meanwhile, the localization results of the PSO, AFSA, and CDNIGS often fall into local optima, leading to abrupt extremum and decreased

positioning accuracy. However, the IAFSA has a relative error less than 1.6% and avoids falling into the local optimum. Obviously, the IAFSA has better location result stability.

#### Influence of Different Time Delay Errors

The theoretical delay  $\tau_{c1}$  of the discharge signal reaching each sensor can be calculated based on the coordinates of each sensor and PD power source, and the speed of electromagnetic waves  $c$ , while the measured delay  $\tau_{i1}$  can be calculated according to the starting time of the first wave. Then the delay measurement error  $\Delta\tau_{i1}$  can be calculated as:

$$\Delta\tau_{i1} = \tau_{i1} - \tau_{c1} \quad (17)$$

According to Equation (15), the experimental data of PD source No.5 in Table 5 was selected to calculate the theoretical delay.

**Table 5.** Localization results and errors for the simulation.

PD Source	CDNIGS <sup>1</sup>			PSO			AFSA			IAFSA		
	Coordinate (mm)	$\Delta_r$ (mm)	$\delta_r$ (%)	Coordinate (mm)	$\Delta_r$ (mm)	$\delta_r$ (%)	Coordinate (mm)	$\Delta_r$ (mm)	$\delta_r$ (%)	Coordinate (mm)	$\Delta_r$ (mm)	$\delta_r$ (%)
1	(1040,650,1230)	140	2.2	(1160,760,1562)	332	5.2	(1195,583,1230)	106	1.7	(1053,609,1337)	<b>91</b>	<b>1.4</b>
2	(1180,200,2080)	340	5.4	(1391,531,2232)	281	4.4	(696,491,2067)	435	6.8	(1088,513,2068)	<b>98</b>	<b>1.5</b>
3	(2700,600,1310)	<b>70</b>	<b>1.1</b>	(2631,532,1192)	162	2.6	(2780,455,1662)	378	5.9	(2829,593,1261)	98	1.5
4	(3960,790,2300)	160	2.5	(3521,752,1826)	527	8.3	(3891,751,2300)	172	2.7	(3838,783,2195)	<b>105</b>	<b>1.6</b>
5	(4810,200,1580)	280	4.4	(4032,421,1509)	582	9.2	(4874,400,2043)	623	9.8	(4623,350,1565)	<b>86</b>	<b>1.4</b>

<sup>1</sup> The position results of the CDNIGS in Table 5 are all from the literature [37]. The bolded content in the table indicates the best experimental results.

Furthermore, the delay errors are artificially added into the theoretical delay to study the influence of different delay errors on the location results. Specific simulation results are shown in Table 6:

From Table 6, when  $\Delta\tau_{il} = 0$  ns, the relative location errors of the three algorithms are all within 1%, and that of the IAFSA is 0.2%. When  $\Delta\tau_{il} = 0.2$  ns, the relative error of the IAFSA becomes 0.5%. Although the location accuracy of the PSO and AFSA is not as high as that of the IAFSA, their relative errors are still less than 1.3%. When  $\Delta\tau_{il} = 0.4$  ns, the PSO and AFSA fall into the local optimum, and the relative error of the IAFSA is 0.6%. When  $0.6$  ns  $< \Delta\tau_{il} < 0.8$  ns, the PSO and AFSA are trapped in the local optimum with relative errors greater than 4.5%, and exceeds 5% when  $\Delta\tau_{il} = 1$  ns. However the maximum relative error of the IAFSA is no more than 1.3%.

With an increase in the delay error, the relative error of the three algorithms also increases. The location results of the PSO and AFSA both show extreme values, but the relative location error of the IAFSA always remains below 1.3%, and there is no extreme value. The delay error partially impacts the location accuracy of the IAFSA. However, within  $\Delta\tau_{il}$  of 1 ns, the IAFSA shows strong robustness, and performs better than the PSO and AFSA in location accuracy.

**Table 6.** Location results with the different delay errors.

$\Delta\tau_{il}/ns$	PSO			AFSA			IAFSA		
	Coordinate (mm)	$\Delta_r$ (mm)	$\delta_r$ (%)	Coordinate (mm)	$\Delta_r$ (mm)	$\delta_r$ (%)	Coordinate (mm)	$\Delta_r$ (mm)	$\delta_r$ (%)
0	(4658,330,1482)	57	0.9	(4630,399,1493)	45	0.7	(4615,368,1484)	<b>10</b>	<b>0.2</b>
0.2	(4647,426,1502)	79	1.2	(4666,301,1507)	85	1.3	(4628,385,1491)	<b>33</b>	<b>0.5</b>
0.4	(4745,552,1555)	247	3.9	(4657,438,1507)	95	1.5	(4627,392,1491)	<b>38</b>	<b>0.6</b>
0.6	(4466,126,1407)	284	4.5	(4782,586,1574)	299	4.7	(4634,403,1494)	<b>52</b>	<b>0.8</b>
0.8	(4680,473,1520)	139	2.2	(4610,49,1481)	311	4.9	(4642,416,1499)	<b>67</b>	<b>1.1</b>
1.0	(4543,692,1455)	340	5.4	(4420,621,1400)	333	5.2	(4585,279,1468)	<b>85</b>	<b>1.3</b>

The bolded content in the table indicates the best experimental results.

## 6. IAFSA for Laboratory PD Location

### Field Experiment

To further verify the effectiveness of the IAFSA, we carried out PD localization experiments in the laboratory. A schematic diagram of PD location is shown in Figure 8. The experimental system consists of GIS, a PD generator, four identical high-frequency sensors, and an oscilloscope. The GIS box is made of stainless steel with a good electromagnetic shielding performance with a length of 3000 mm and a radius of 300 mm, as shown in Figure 9. The coordinates of the four high-frequency sensors are  $S_1$  (0,450,600),  $S_2$  (300,1650,300),  $S_3$  (300,1950,300), and  $S_4$  (0,2250,600) mm, and  $S_1$  is the reference sensor. The power–frequency high-voltage control platform is used to apply high voltage (10 kV) to a PD defective model to generate a PD signal. The sensor used in the experiment was a microwave antenna. A front RF amplifier was internally designed. Before signal transmission, the RF was amplified to improve the signal-to-noise ratio. The gain of the amplifier was set at 10 dB. A high-pass filter was built into the channel to filter out interference signals. The detection frequency band of the sensor was 100 to 1500 MHz. An oscilloscope was used to collect the resultant signals. The system adopts the dsox4154a-type digital storage oscilloscope of the Keysight Technologies company. The four channels of the oscilloscope can be simultaneously acquired. When the four channels are synchronized, the acquisition frequency of each channel can reach 1.5 GHz, and the acquisition rate is 5 GS per second. When measuring, the oscilloscope can be directly connected to the PC terminal, and the collected waveform data is stored on the PC terminal to facilitate subsequent analysis.

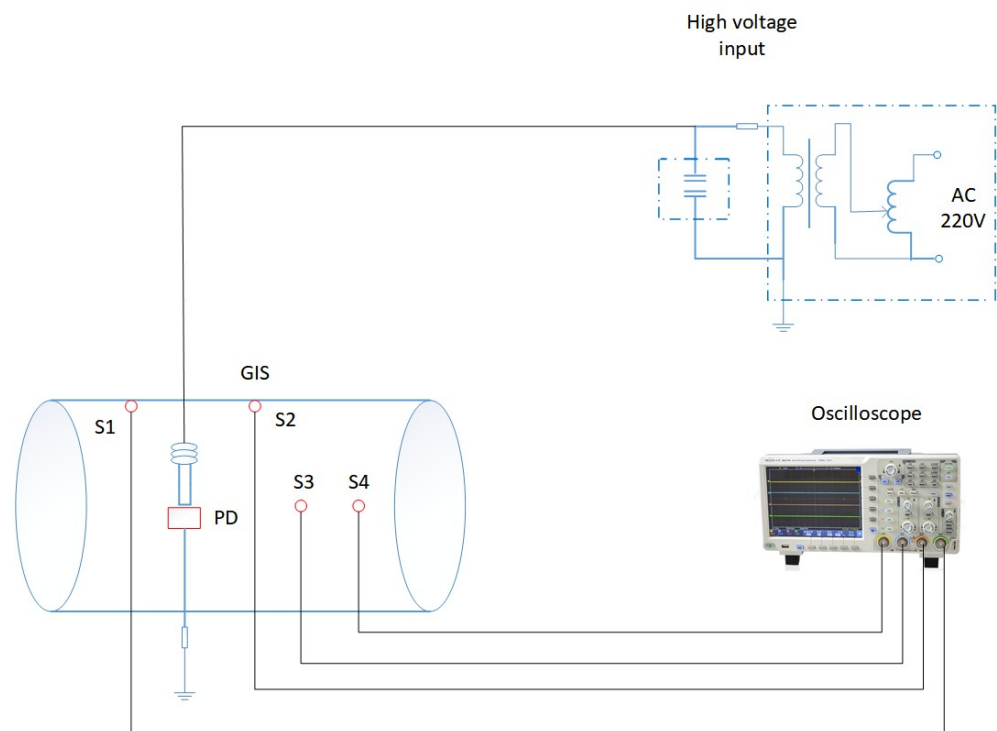


**Figure 8.** Schematic diagram of the localization-based position system.

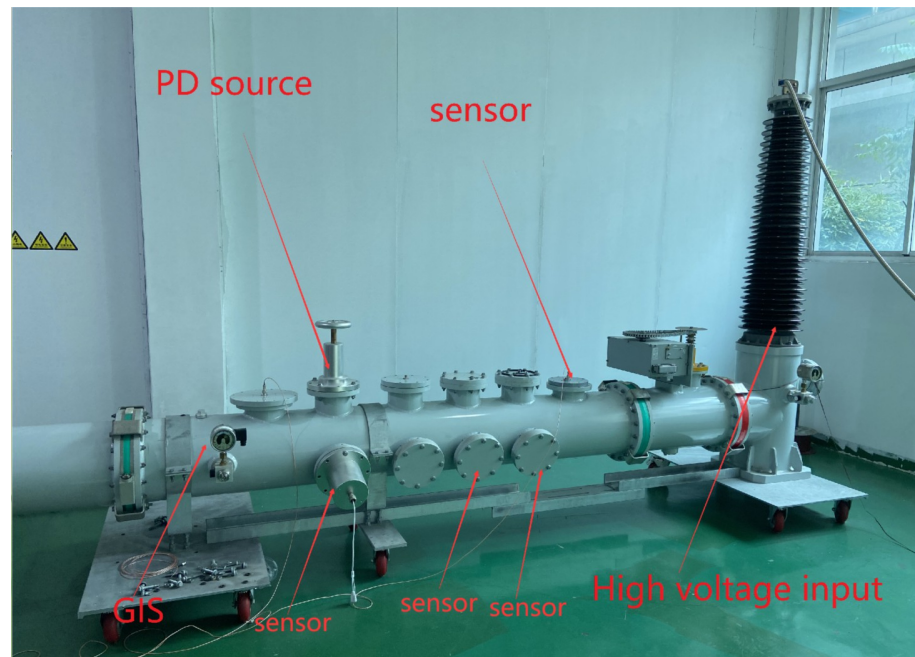


Figure 9. Layout and localization diagram.

The curves of the four waveforms in Figure 10 correspond to the local discharge signals received by the four sensors in Figure 8, and the local discharge signals were received by the sensors at  $-8$  ns. These waveforms were obtained by shifting the oscilloscope up and down to more intuitively observe the time delay of the signals received by the sensors located at different positions. The horizontal axis in the figure represents time, with each small grid representing 20 ns, while the vertical axis represents the voltage amplitude, with each small grid representing 200 mV.

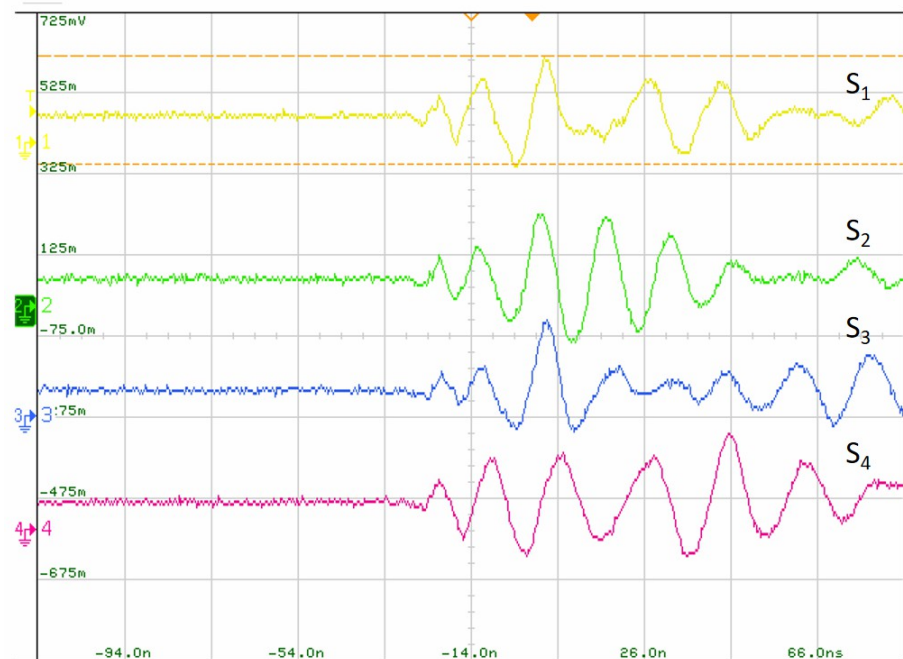
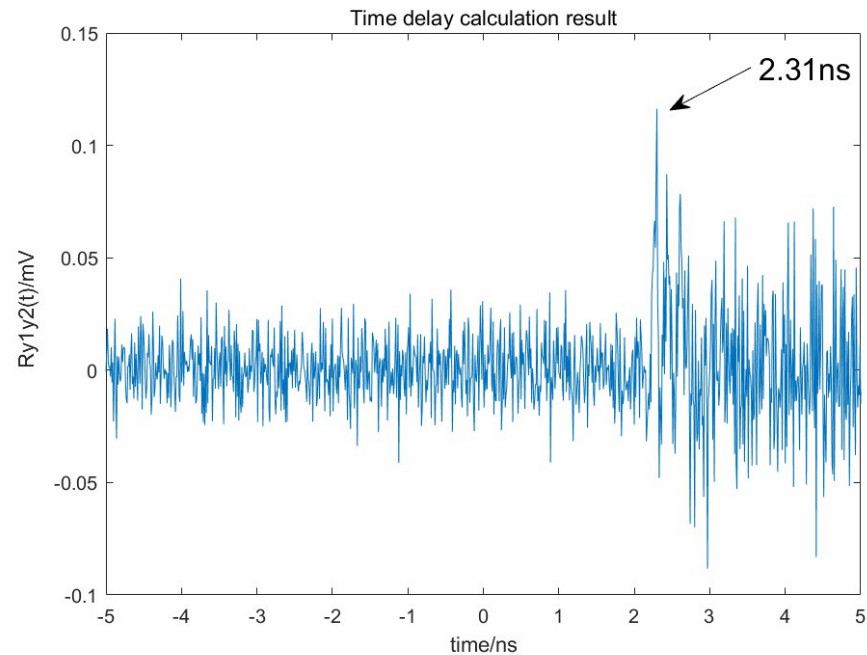


Figure 10. Actual PD signals.

After collecting the waveform data by the four-channel oscilloscope, the time delay was calculated by the GCC algorithm. The Hassab-Boucher (HB) weighting method was adopted with the weighting function of  $|G_{x_1x_2}|(G_{x_1x_1}G_{x_2x_2})^{-1}$ , suppressing the periodic

component of the signal. At low SNR values, the effect is similar to that of the direct cross-correlation method, and the estimation accuracy is high. Figure 11 is the time delay calculation results of the field experiment. The data collected by  $S_3$  and  $S_1$  in the first experiment was selected and the time delay  $\tau_{31}$  calculated. The peak position in Figure 11 is 2.31 ns, implying that the time delay is 2.31 ns. The other time delays were obtained by this method.



**Figure 11.** Time delay obtained the by HB weighting method.

The theoretical delays, measured delays and delay errors of the five PD sources are shown in Table 7.

In Table 7, the minimum and maximum delay errors are 0.03 and 0.51 ns, respectively. This indicates that the time delay accuracy obtained by the GCC with the HB weighted method can be used for PD localization.

**Table 7.** Theoretical time delay, measured time delay, and time delay errors of the five PD sources.

PD Source	Coordinate of PD (mm)	Theoretical Delay (ns)	Measured Delay (ns)	Delay Error (ns)
1	(0,900,400)	1.07, 2.01, 2.91	1.14, 2.31, 2.94	0.07, 0.30, 0.03
2	(0,1350,500)	−1.45, −0.69, 0.00	−1.51, −0.83, 0.21	−0.06, −0.14, 0.21
3	(100,900,300)	0.75, 1.73, 2.79	1.01, 1.70, 2.84	0.26, −0.03, 0.05
4	(100,1050,300)	−0.15, 0.81, 1.88	−0.22, 0.96, 1.92	−0.07, 0.15, 0.04
5	(100,1350,300)	−1.98, −1.07, 0.00	−2.41, −0.56, 0.26	−0.43, 0.51, 0.26

Using the measured time delay, the localization calculation can be carried out. To compare the location effects, the parameters of the PSO, AFSA and IAFSA are set in Table 8.

**Table 8.** Parameter settings of each algorithm for laboratory.

Algorithm	$K_{max}$	N	Step <sub>1</sub>	Visual <sub>1</sub>	$\delta$	trynumber	$\omega$	$c_1 = c_2$
PSO	60	80	—	—	—	—	0.6	2
AFSA	60	80	8	6	0.618	30	—	—
IAFSA	60	80	8	6	0.618	30	—	—

The position results and errors of the three algorithms are shown in Table 9. From Table 9, we can reach the following conclusions. Firstly, when the delay error is small,

the localization results of the three algorithms are relatively stable, and there are no extreme values or local optima. However, when the delay error is large, the localization results of the PSO and AFSA both fall into local optima and exhibit extreme values, while the positioning error of the IAFSA is controlled within 2.4%, and the localization results are relatively stable. Secondly, in terms of the comprehensive localization error, the localization effect of the IAFSA is superior to that of the AFSA and PSO. The IAFSA can achieve strong globality and stability in localization, with relative positioning errors all within 2.4%, meeting the requirements of precise on-site positioning.

**Table 9.** Localization results and errors from laboratory experiments.

PD Source	PSO			AFSA			IAFSA		
	Coordinate (mm)	$\Delta_r$ (mm)	$\delta_r$ (%)	Coordinate (mm)	$\Delta_r$ (mm)	$\delta_r$ (%)	Coordinate (mm)	$\Delta_r$ (mm)	$\delta_r$ (%)
1	(137,905,540)	196	6.4	(78,902,457)	97	3.1	(49,905,404)	<b>49</b>	<b>1.6</b>
2	(8,1362,590)	92	3.0	(36,1350,456)	<b>57</b>	<b>1.8</b>	(13,1345,557)	59	1.9
3	(105,864,200)	105	3.4	(36,878,190)	128	4.1	(135,904,343)	<b>56</b>	<b>1.8</b>
4	(72,1044,253)	54	1.7	(84,1046,271)	32	1.0	(89,1046,275)	<b>26</b>	<b>0.8</b>
5	(255,1717,392)	409	13.2	(296,1664,126)	409	13.2	(72,1348,230)	<b>74</b>	<b>2.4</b>

The bolded content in the table indicates the best experimental results.

## 7. Conclusions

The traditional AFSA has the disadvantages of a slow convergence speed and can easily fall into a local optimum in the late stage; therefore, the optimal solution cannot meet the actual engineering requirements when the AFSA is applied in PD localization. In this paper, a 3D TDOA localization algorithm based on the IAFSA is proposed. Firstly, the detection behaviour of the ABC is introduced into the AFSA, improving its ability to jump out of local extremum and global search, overcoming the premature phenomenon. Secondly, the adaptive vision field and step length are adopted. In the early stage of the search, the search-ability of the global optimal solution and convergence speed are improved by increasing the vision field and step length. In the middle stage, the vision field and step length are gradually reduced to find the local optimal solution. In the late stage, the vision field and step length are reduced to a minimum, and the search focuses in the remaining small area with greatly improved optimization accuracy. Finally, the IAFSA is applied to PD localization. Simulation and field experiment results show that the IAFSA has a better localization performance than the AFSA or PSO.

Compared with popular algorithms such as neural networks and deep learning, the IAFSA does not require a large amount of data to train the model; it does not require powerful computing resources to run, unlike neural networks and deep learning; and it has low hardware requirements, running on portable devices such as embedded systems making it highly practical. Regarding future research directions, one potential avenue is the use of high-speed AD acquisition chips to replace oscilloscopes and store acquired data on embedded platforms, such as FPGAs. Another possibility is to combine the positioning system with a smart inspection robot for GIS substations using 5G communication, in order to achieve fully automated and intelligent localization of partial discharge sources in substations.

**Author Contributions:** Conceptualization, H.Q. and Q.W.; methodology, H.Q., Q.W., H.N.; software, Q.W.; validation, H.Q., Q.W. and J.Z.; formal analysis, Q.W. and Z.W.; investigation, Q.W. and H.N.; resources, H.Q. and J.Z.; data curation, Q.W., H.N. and J.Z.; writing—original draft preparation, Q.W.; writing—review and editing, H.Q. and Q.W.; visualization, Q.W.; supervision, H.Q. and J.Z.; All authors have read and agreed to the published version of the manuscript.

**Funding:** This research was funded by the Postgraduate Research & Practice Innovation Program of Jiangsu Province under the grant number [SJCX21\_1283].

**Data Availability Statement:** Not applicable.

**Conflicts of Interest:** The authors declare no conflicts of interest.

### Abbreviations

The following abbreviations are used in this manuscript:

TDOA	Time difference of arrival
IAFSA	Improved artificial fish swarm algorithm
ABC	Artificial bee colony
AFSA	Artificial fish swarms algorithm
PSO	Particle swarm optimization
GIS	Gas-insulated switchgear
PD	Partial discharge
TOA	Time of arrival
AOA	Angle of arrival
RSS	Received signal strength
TR	Time reversal
RSS	Received signal strength
WPT	Wavelet packet transform
UHF	Ultra-high frequency
HF	High-frequency
CC	Cross-correlation
GCC	Generalized cross-correlation
HB	Hassab–Boucher
CDNIGS	Complex domain Newton iteration-grid search method

### References

- Zang, Y.; Qian, Y.; Wang, H.; Xu, A.; Zhou, X.; Sheng, G.; Jiang, X. A Novel Optical Localization Method for Partial Discharge Source Using ANFIS Virtual Sensors and Simulation Fingerprint in GIL. *IEEE Trans. Instrum. Meas.* **2021**, *70*, 3522411. [[CrossRef](#)]
- Li, X.; Wang, X.; Yang, A.; Rong, M. Partial Discharge Source Localization in GIS Based on Image Edge Detection and Support Vector Machine. *IEEE Trans. Power Deliv.* **2019**, *34*, 1795–1802. [[CrossRef](#)]
- Darwish, A.; Refaat, S.S.; Abu-Rub, H.; Toliyat, H.A. PD Signal Propagation in GIS: Ultra-High Frequency Detection-Based Modeling. *IEEE Sens. J.* **2020**, *20*, 9417–9426. [[CrossRef](#)]
- Dhara, S.; Koley, C.; Chakravorti, S. A UHF Sensor Based Partial Discharge Monitoring System for Air Insulated Electrical Substations. *IEEE Trans. Power Deliv.* **2021**, *36*, 3649–3656. [[CrossRef](#)]
- Polužanski, V.; Kartalović, N.; Nikolić, B. Impact of power transformer oil-temperature on the measurement uncertainty of all-acoustic non-iterative partial discharge location. *Materials* **2021**, *14*, 1385. [[CrossRef](#)] [[PubMed](#)]
- Perfetto, L.; D’antona, G. Experimental results of partial discharge localization in bounded domains. *Sensors (Switzerland)* **2021**, *21*, 935. [[CrossRef](#)] [[PubMed](#)]
- Nobrega, L.A.; Costa, E.G.; Serres, A.J.; Xavier, G.V.; Aquino, M.V. UHF partial discharge location in power transformers via solution of the maxwell equations in a computational environment. *Sensors* **2019**, *19*, 3435. [[CrossRef](#)]
- Judd, M.D. Experience with UHF partial discharge detection and location in power transformers. In Proceedings of the 2011 Electrical Insulation Conference (EIC), Annapolis, MD, USA, 5–8 June 2011; pp. 201–205.
- Xie, Q.; Cheng, S.; Lü, F.F.; Li, Y. Location of partial discharge in transformer oil using circular array of ultrasonic sensors. *IEEE Trans. Dielectr. Electr. Insul.* **2013**, *20*, 1683–1690. [[CrossRef](#)]
- He, L.; Li, S.; Zhou, D.; Ding, D.; Wang, J.; Ma, X. Analysis method of abnormal condition in GIS based on ultrasonic detection. In Proceedings of the 2016 International Conference on Condition Monitoring and Diagnosis (CMD), Xi’an, China, 25–28 September 2016; pp. 570–573. [[CrossRef](#)]
- Li, J.; Li, X.; Du, L.; Cao, M.; Qian, G. An intelligent sensor for the ultra-high-frequency partial discharge online monitoring of power transformers. *Energies* **2016**, *9*, 383. [[CrossRef](#)]
- Mohd Hashim, A.H.; Azis, N.; Jasni, J.; Mohd Radzi, M.A.; Kozako, M.; Kamarol Mohd Jamil, M.; Yaakub, Z. Partial Discharge Localization in Oil Through Acoustic Emission Technique Utilizing Fuzzy Logic. *IEEE Trans. Dielectr. Electr. Insul.* **2022**, *29*, 623–630. [[CrossRef](#)]
- Iorkyase, E.T.; Tachtatzis, C.; Atkinson, R.C.; Glover, I.A. Localisation of partial discharge sources using radio fingerprinting technique. In Proceedings of the 2015 Loughborough Antennas and Propagation Conference (LAPC), Loughborough, UK, 2–3 November 2015; pp. 1–5. [[CrossRef](#)]
- Chai, H.; Phung, B.T.; Mitchell, S. Application of UHF sensors in power system equipment for partial discharge detection: A review. *Sensors* **2019**, *19*, 1029. [[CrossRef](#)] [[PubMed](#)]

15. Roslizan, N.; Rohani, M.; Wooi, C.; Isa, M.; Ismail, B.; Rosmi, A.; Mustafa, W. A review: Partial discharge detection using UHF sensor on high voltage equipment. In *Proceedings of the Journal of Physics: Conference Series*; IOP Publishing: Bristol, UK, 2020; Volume 1432, p. 012003.
16. de Andrade Lira, R.V.; de Siqueira Campos, A.L.P.; Neto, A.G.; Junior, I.d.S.S.; Serres, A.J.R.; Nobrega, L.A.M.M.; da Costa Silva, A.D.; Carvalho, I.F. Elliptical UHF sensor for partial discharge detection. *Sensors Actuators A Phys.* **2022**, *348*, 113981. [[CrossRef](#)]
17. Wang, X.; Niu, B.; Hu, B.; Jin, H.; Wu, Z.; Wang, D. Research on Partial Discharge Source Positioning in Switchgear Based on PSO. In *Proceedings of the 2021 International Conference on Electrical Materials and Power Equipment (ICEMPE)*, Chongqing, China, 11–15 April 2021; pp. 1–4.
18. Delivopoulos, E.; Theocharis, J.B. A modified PNN algorithm with optimal PD modeling using the orthogonal least squares method. *Inf. Sci.* **2004**, *168*, 133–170. [[CrossRef](#)]
19. Du, R.; Jiang, L.; Liu, S.; Li, W.; Bian, X.; Chen, L.; Si, W. Application of Genetic Algorithm in PD Source Location in Transformer Oil. In *Proceedings of the 2020 5th International Conference on Smart Grid and Electrical Automation (ICSGEA)*, Zhangjiajie, China, 13–14 June 2020; pp. 1–5.
20. Meka, K.C.; Giridhar, A.; Siva Sarma, D. PD Source Location Utilizing Acoustic TDOA Signals in Power Transformer by Fuzzy Adaptive Particle Swarm Optimization. *Radioengineering* **2018**, *27*, 1119–1127. [[CrossRef](#)]
21. Zhang, X.; Tang, J.; Xie, Y. Taylor-genetic Algorithm on PD Location. In *Proceedings of the 2008 International Conference on High Voltage Engineering and Application*, Chongqing, China, 9–12 November 2008; pp. 685–688.
22. Cai, J.; Zhou, L.; Hu, J.; Zhang, C.; Liao, W.; Guo, L. High-accuracy localisation method for PD in transformers. *IET Sci. Meas. Technol.* **2020**, *14*, 104–110. [[CrossRef](#)]
23. Dhara, S.; Koley, C.; Chakravorti, S. Methods for localization of partial discharge sources within air insulated electrical substation. In *Proceedings of the 2018 20th National Power Systems Conference (NPSC)*, Tiruchirappalli, India, 14–16 December 2018; pp. 1–6.
24. Forestiero, A. Heuristic recommendation technique in Internet of Things featuring swarm intelligence approach. *Expert Syst. Appl.* **2022**, *187*, 115904. [[CrossRef](#)]
25. Forestiero, A.; Mastroianni, C.; Spezzano, G. Reorganization and discovery of grid information with epidemic tuning. *Future Gener. Comput. Syst.* **2008**, *24*, 788–797. [[CrossRef](#)]
26. Li, M.; Feng, X.; Man, X. A method based on TDOA and TS - PSO to UHF partial discharge location in transformers. *Proc. CSEE* **2019**, *39*, 9.
27. Gardner, W.; Spooner, C. Comparison of autocorrelation and cross-correlation methods for signal-selective TDOA estimation. *IEEE Trans. Signal Process.* **1992**, *40*, 2606–2608. [[CrossRef](#)]
28. Grigorie, T.L.; Corcau, J.I.; Lungu, M.; Sandu, D.G. Bi-dimensional position detection using TDOA estimation through cross correlation of the acoustic signals. Part 1: Theoretical background. In *Proceedings of the 2009 7th International Conference on ICT and Knowledge Engineering*, Bangkok, Thailand, 1–2 December 2009; pp. 28–32. [[CrossRef](#)]
29. Azizi, R. Empirical study of artificial fish swarm algorithm. *arXiv* **2014**, arXiv:1405.4138.
30. Neshat, M.; Sepidnam, G.; Sargolzaei, M.; Toosi, A.N. Artificial fish swarm algorithm: A survey of the state-of-the-art, hybridization, combinatorial and indicative applications. *Artif. Intell. Rev.* **2014**, *42*, 965–997. [[CrossRef](#)]
31. Pourpanah, F.; Wang, R.; Lim, C.P.; Wang, X.Z.; Yazdani, D. A review of artificial fish swarm algorithms: Recent advances and applications. *Artif. Intell. Rev.* **2023**, *56*, 1867–1903. [[CrossRef](#)]
32. Zhang, C.; Zhang, F.M.; Li, F.; Wu, H.S. Improved artificial fish swarm algorithm. In *Proceedings of the 2014 9th IEEE Conference on Industrial Electronics and Applications*, Hangzhou, China, 9–11 June 2014; pp. 748–753.
33. Karaboga, D.; Gorkemli, B.; Ozturk, C.; Karaboga, N. A comprehensive survey: Artificial bee colony (ABC) algorithm and applications. *Artif. Intell. Rev.* **2014**, *42*, 21–57. [[CrossRef](#)]
34. Bolaji, A.L.; Khader, A.T.; Al-Betar, M.A.; Awadallah, M.A. Artificial bee colony algorithm, its variants and applications: A survey. *J. Theor. Appl. Inf. Technol.* **2013**, *47*.
35. Sharma, A.; Sharma, A.; Choudhary, S.; Pachauri, R.K.; Shrivastava, A.; Kumar, D. A review on artificial bee colony and its engineering applications. *J. Crit. Rev.* **2020**, *7*, 4097–4107.
36. Zheng, J.; Gao, Y.; Zhang, H.; Lei, Y.; Zhang, J. OTSU Multi-Threshold Image Segmentation Based on Improved Particle Swarm Algorithm. *Appl. Sci.* **2022**, *12*, 11514. [[CrossRef](#)]
37. Zheng, S.; Li, C.; He, M. Newton iterative grid search method in complex field for partial discharge of transformer. *Proc. CSEE* **2019**, *33*, 155–161.

**Disclaimer/Publisher’s Note:** The statements, opinions and data contained in all publications are solely those of the individual author(s) and contributor(s) and not of MDPI and/or the editor(s). MDPI and/or the editor(s) disclaim responsibility for any injury to people or property resulting from any ideas, methods, instructions or products referred to in the content.